CHAPTER 5

TWO-DIMENSIONAL ANGLE MEASURE TECHNIQUE FOR IMAGE TEXTURE ANALYSIS

JESPER BRØNDUM

SUBMITTED TO PATTERN RECOGNITION

ABSTRACT

The angle measure technique (AMT) has recently been adapted from characterisation of geomorphic complexity to image texture analysis of uni-lateral illuminated images. In this paper, the AMT is extended to two-dimensional texture image analysis. AMT transforms an intensity and scale dependent angle between two vectors in the spatial domain to the scale domain. By averaging the angle over N repetitions, a mean angle is obtained for a specific scale value. The scale is varied, and a spectrum displaying the average angle in the scale domain is obtained. Using multivariate data analysis with the either Tucker decomposition or multi-way partial least squares regression, the AMT data is further processed. With three different sampling constraints in the spatial domain, three modes are developed: 1) random sampling, 2) direction dependency, and 3) rotational independency. The 2D-AMT is illustrated on a simple 2D sinusoid image, and applied successfully to two specific problems: classification of the Brodatz natural textures and prediction of intramuscular fat in ultrasound images. The AMT is advantageous in the lack of required optimisation due to the few parameters influencing the AMT data and the possibility of mapping texture information from images of different sizes and even different dimensions onto the same domain for comparison.

INTRODUCTION

Texture analysis is in many computer vision applications one of the primary tasks. Among the approaches that have been taken in texture studies are frequency domain features[1] and Gabor filters[2], texture filters[3], fractal models[4], wavelets[5], and the widely used co-occurrence matrix features[6]. Reviews of texture approaches are given by Buf *et al.*[7] and Reed *et al.*[8]. The latter proposed a coarse grouping of texture feature extraction techniques into feature-based, model-based, and structural. Generally, all the approaches do, however, suffer from being dependent on a parametric optimisation and scale.

In 1994 Andrle[9] introduced the Angle Measure Technique (AMT) for characterisation of geomorphic complexity. Prior to the paper by Andrle, the favoured method for landscape characterisation was the fractal dimension, but this method suffers from the assumption of constant complexity over some range of scale. Therefore, Andrle proposed the AMT, which introduced a map of complexity with the scale dimension, and consequently eliminated the assumption of a constant complexity.

Esbensen *et al.*[10] adopted the AMT as a way to texture transform images to the scale domain as a non-recursive analogy to the Fourier transformation. In the approach by Esbensen *et al.* approach, images acquired with unilateral illumination at 10-15° relative to the scene were unfolded to one dimension (e.g. a 256×256 image is unfolded into a 65,536 vector) and measured with the same approach as Andrle. Esbensen and co-workers further extended the AMT by introducing a mean intensity variable in the scale domain along with the angle variable. The spectral output in the scale domain was used in multivariate data analysis. Whether the data analysis was applied for classification or prediction, the texture features (represented by the AMT spectra) were practically non-parametric. In the further work of Kvaal *et al.*[11], the AMT spectra from bread were used to predict sensory panel scores with superior results compared to SVD texture features developed by Kvaal *et al*.[12].

The one-dimensional AMT extracts information from one direction in the image only due to the unfolding and potential neighbouring information is thus neglected. In this paper, a two-dimensional extension to the 1D-AMT is proposed. Three approaches to this are made based on the sampling properties in the spatial domain: 1) a random sampling, 2) directional dependency, and 3) rotational independency. The approaches still suffer from being non-recursive like the 1D-AMT, but do present a more extensive utilisation of the neighbouring information than the simple image unfolding.

The AMT is very user friendly since it involves practically no parameters to be set by the user. By involving decomposition techniques like Principal Component Analysis [13], Tucker [14,15].

AMT can be further extended into unsupervised classification as is illustrated in this paper. A brief introduction to the one-dimensional AMT including the mathematical definition is given. This is followed by a description of the two-dimensional AMT technique.

The AMT texture features are applied to three types of images: artificial two-dimensional sinusoid images, unsupervised classification of the Brodatz textures, and prediction of intramuscular fat from biological ultrasound images.

ONE-DIMENSIONAL ANGLE MOMENT TRANSFORMATION (MODE 0)

As mentioned earlier, the initial approach for image texture analysis with AMT was performed on unfolded images. Figure 1a illustrates the principle of the 1D-AMT, which throughout the paper will be denoted Mode 0. The curve represents the signal, which can be a geometric line, a spectrum, or image unfolded to one dimension. The point origo, denoted by the *O*, is found randomly on the curve. The *A* and *B* points are found at the exact distance *s* from *O*. *s* is the scale variable, and is increased in an iterative process from a minimum to a maximum value. The increment can be either linear or in specific steps. The angle between the vectors $\overline{OA}$ and $\overline{OB}$ is denoted α. In the original proposal by Andrle, the complement to α was used, but for practical reasons α will be used instead as also proposed by Esbensen[10]. The procedure is repeated *N* times for each s value. Averaging the *N* values of α result in a Mean Angle *MA*. Thus, for a given value of *s* the AMT parameter MA_s is found as the mean angle between the two vectors $\overline{O_i A_{i,s}}$ and $\overline{O_i B_{i,s}}$ as shown in equation 1.

$$MA_s = \frac{1}{N}\sum_{i=1}^{N} \alpha\left(\overline{O_i\ A_{i,s}}, \overline{O_i\ B_{i,s}}\right) \tag{1}$$

where $\alpha(v_1, v_2)$ determines the minimum angle between the two vectors v_1 and v_2.

Esbensen *et al.*[10] also proposed to use the mean value of the intensity difference between the $A_{i,s}$ and $B_{i,s}$ points, denoted *MY*, as shown in equation 2.

$$MY_s = \frac{1}{N}\sum_{i=1}^{N} \left| I(A_{i,s}) - I(B_{i,s}) \right| \tag{2}$$

where *I(A)* denote the signal intensity of the point *A*.

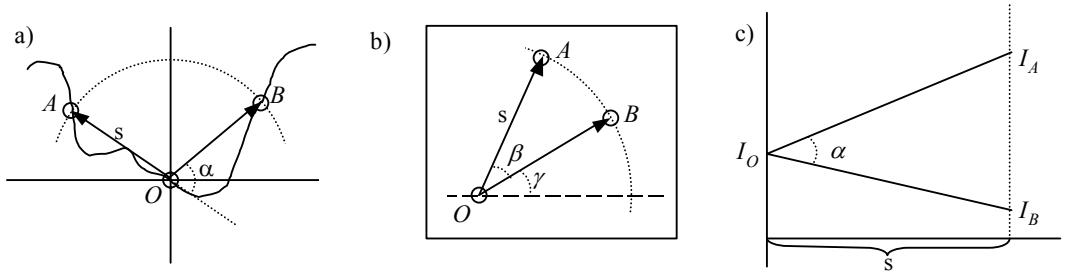

Figure 1. Overview of the AMT Principle. a) the one-dimensional AMT, b) selection of points in the two-dimensional AMT, c) calculation of MA and MY in the scale domain.

TWO-DIMENSIONAL AMT (MODE 1-3)

The two-dimensional AMT is implemented on the entire image instead of working on the unfolded image only. Figure 1b illustrates this situation with an image canvas. The origo, O, is selected randomly in the image. The two points A and B are found in the image at a spatial distance s from O. A and B are also selected with the constraint that the spatial angle between the two vectors $\overline{OA}$ and $\overline{OB}$ is β. Furthermore, the angle between $\overline{OA}$ and the horizontal direction in the image is γ.

Three different approaches for sampling the points in the spatial domain are proposed and these approaches will be denoted Mode 1-3 throughout the paper. The modes possess specific characteristics regarding the sampling method: Mode 1 samples the A and B points randomly in the spatial domain, Mode 2 sample A and B with a directional dependency, and Mode 3 samples A and B in rotational invariant manner. In all three two-dimensional modes, O is selected randomly in the image. Once O, A, and B are selected in the image, the angle α and the intensities of the points $I(O)$, $I(A)$, and $I(B)$ can be mapped onto the scale domain as depicted in Figure 1c.

MODE 1. RANDOM SAMPLING

In the random sampling approach, β is simply selected randomly. In the current implementation, β is selected between 0°, 45°, 90°, and 135°, but the selection principle can easily be made with a higher resolution. The angle, γ, between the two vectors, is constantly set to 180°. Thus, the A and B points are now depending on both the scale s and on β. Letting O^*, A^* and B^* denote O, A, and B in the scale domain (see Figure 1c) equation 1 can now be substituted into equation 3.

$$MA_{s,\beta} = \frac{1}{N}\sum_{i=1}^{N} \alpha\left(\overline{O_i^* \; A_{i,s,\beta}^*}, \overline{O_i^* \; B_{i,s,\beta}^*}\right) \tag{3}$$

Similarly *MY* can be calculated as shown in Equation 4.

$$MY_{s,\beta} = \frac{1}{N}\sum_{i=1}^{N}\left|I(A^*_{i,s,\beta}) - I(B^*_{i,s,\beta})\right| \quad (4)$$

MODE 2. DIRECTIONAL DEPENDENCY

In the directional dependency approach, the AMT spectrum is calculated for a number of different values of β and with γ=180°. Thereby the output is two-dimensional where the first dimension represents the scale dimensions and the second represents the β dimension. Again, β is in the current application calculated for values of 0, 45, 90, and 135 only, but could easily be implemented with a higher resolution. In images with textural different patterns in the different textural directions, the AMT spectra are expected to differ for the different β values. *MA* and *MY* are calculated using O^*, A^* and B^* as shown in equation 3 and 4.

MODE 3. ROTATIONAL INDEPENDENCY

The Mode 3 approach introduces a constraint on the angle, γ, between the $\overline{O_i A_{i,s}}$ and $\overline{O_i B_{i,s}}$ vectors (see Figure 1b). So far γ has been constant (here it has been set to 180°), but to obtain robustness towards rotation of the image, γ is now used as the second dimension of the AMT data. The approach here is to select *O* randomly in the image, and then select *A* randomly at the distance *s* from *O*. Thus, the position of *B* is found at *s* and γ. Gamma is here chosen to be 0°, 45°, 90°, and 135° but similar to the conditions for β in Mode 2, the interval can easily be modified to represent a higher resolution. *MA* and *MY* are calculated as shown in Equation 3 and 4.

MULTIVARIATE PROCESSING OF THE AMT DATA

Processing the AMT data is done using multivariate techniques. Due to the spectral conditions of the AMT data, traditional statistics are not appropriate because of the co-linearity of the data. Multivariate methods are efficient for decomposing the co-linear data into a common structure and work on the decomposed data. Two multivariate methods are used here, namely the Tucker3 decomposition for classification and N-way Partial Least Squares (N-PLS) for regression. The N-way techniques are quite recent in linear data analysis, where the common approach have been to work on unfolded data and thereby ignore the combination of the different dimensions[16]. Better interpretation, decomposition and occasionally predictions from multivariate data seem to favour the true N-way techniques when working with N-way data[15].

Tucker decomposition. An approach to decompose a three-way data array was introduced by Tucker[17,18]. The method is widely known as a three-way principal component analysis[15] and has later been adapted to the N-way domain. In the three-way example the AMT data is kept in a three-dimensional array ***X*,** with the measured samples in the rows and the AMT data in the two other dimensions. The decomposition results in a number of loadings for each of the variable dimensions. With the Tucker approach, this number can be selected specifically for each dimension. A matrix representation of the three-way model of the Tucker decomposition can be expressed as shown in Equation 5.

$$X = TG(W_1 \otimes W_2)^T + E \tag{5}$$

where ⊗ denotes the Kronecker tensor product. ***T*** denotes a decomposed score matrix, where each sample is represented by one value for each decomposed factor. $\boldsymbol{W_1}$ is a loading in the first dimension (e.g. the scale dimension for the AMT data). If the decomposition in the Tucker model is made using SVD, the loadings are orthogonal and the loadings therefore reproduce the original information contained in ***X*** with much fewer variables. $\boldsymbol{W_2}$ is the corresponding loading in the second dimension. ***G*** is a socalled core array describing the interaction between the loadings. ***E*** denotes the remaining error after the decomposition. The Tucker model has rotational freedom and the decomposition is therefore not unique. A discussion of this problem and the entire algorithm for the Tucker model can be found in Bro[15].

N-PLS is a recently developed multivariate regression approach proposed by Bro[19] dealing with regression of multi-way data. Again, the AMT data is kept in the N-way array ***X*** and the reference data, to be predicted from ***X***, is represented by the vector ***y***. N-PLS performs a decomposition of ***X*** by ensuring maximal covariance between ***X*** and ***y***. The model of the N-PLS method is shown in equation 6.

$$X = T(W_1 |\otimes| W_2)' + E \tag{6}$$

where |⊗| denotes the Khatri-Rao product[20]. W_1 and W_2 are the common structures of the two feature dimensions called the weight vectors (similar to the loadings for the Tucker model). Again ***T*** contains the scores of the decomposed features for the measured samples. Combining the ***T*** matrix and the ***y*** vector, the regression coefficients of the decomposed features can be found. For more information on the principle and the algorithm the please refer to Bro[15,19].

RESULTS

APPLICATION 1. TWO-DIMENSIONAL SINUSOID IMAGE

An artificially created demonstration image, shown in Figure 2, is generated from 8 horizontal and 16 vertical sinusoids on a 256×256 canvas. The AMT data is measured with s ranging from 1 to 30 in single steps, with N =1000. The *MA* data for all four modes are shown in Figure 3a, 3c, and 3e, and *MY* are shown in Figure 3b, 3d, and 3f. *MA* for Mode 0 shows the delimitation by using the unfolded image data, as only the vertical sinus (with a period of 32 pixels). As expected, half the sampling period, s=16, results in an *MA* of 0. *MA* of Mode 1 also represents the vertical sinusoids (with a period of 16 pixels), and local minima of *MA* are observed at s=8, 16 and 24. Figure 3c shows *MA* of Mode 2 for all four values of β. For β=0, the results corresponds to the data obtained for Mode 0. *MA* for β=45° and β=135° are as expected practically similar for the sinusoids. *MA* for β=90° corresponds to measuring the unfolded image vertically, and *MA* values of 0 are observed a scale values of 8, 16, and 24. Figure 3e shows *MA* of Mode 3 for all four values of γ. The *MA* data for γ=180° equals *MA* for Mode 0 as expected. For low s-values the *MA* for γ=45° are smaller than for the larger γ angles. The *MY* data for Mode 0, Mode 2 with β=0°, and Mode 3 with γ=180° results in a curve shape similar to the absolute value of the sine curve and with the same frequency. Local minima are observed at s values of 8, 16, and 24 similar to the observations made for *MA*.

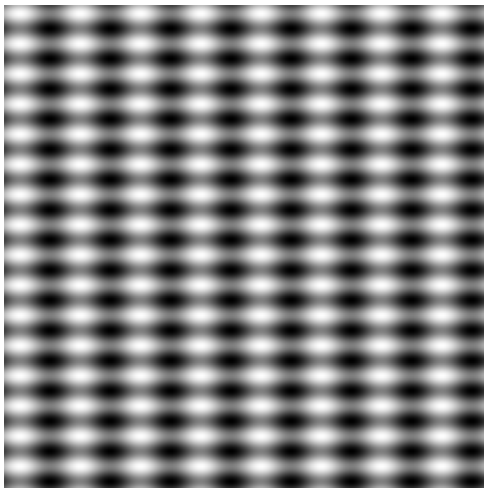

Figure 2. Test image with 2D sinusoids. The image is constructed of 8 horizontal and 16 vertical sinusoids.

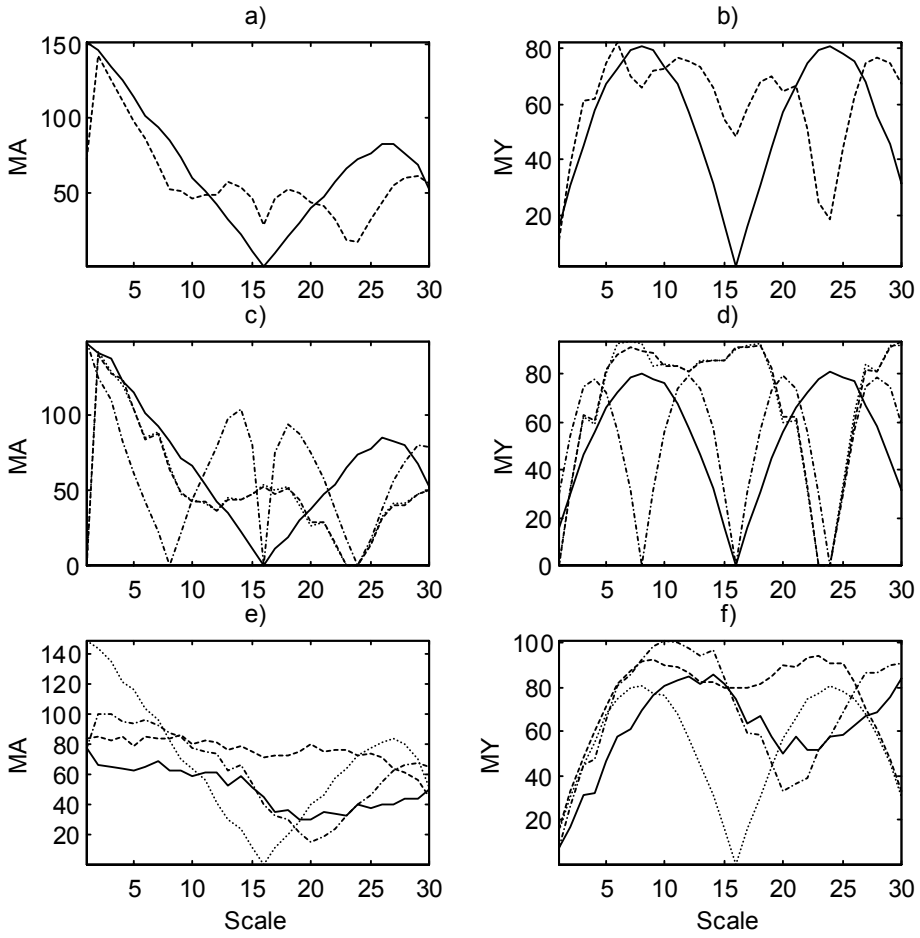

Figure 3. AMT data of the sinusoid image shown in Figure 2. a) MA for Mode 0 (—) and Mode 1 (– –). b) MY for Mode 0 (—) and Mode 1 (– –). c) MA for Mode 2, β=0° (—), β=45° (– –), β=90° (– · –), β=135° (----). d) MY for Mode 2, β=0° (—), β=45° (– –), β=90° (– · –), β=135° (----). e) MA for Mode 3, γ=45° (—),γ=90° (– –), γ=135° (– · –), γ=180° (----). f) MY for Mode 3, γ=45° (—),γ=90° (– –), γ=135° (– · –), γ=180° (----).

APPLICATION 2. CLASSIFICATION OF BRODATZ TEXTURE IMAGES

The natural textures from Brodatz[21]are widely used in texture studies[2] [22], and have been proposed as a standard method for testing new texture techniques[7]. The textures are available digitized from e.g. ftp://freebie.engin.umich.edu/pub/misc/textures. Six of the texture images are shown in Figure 4 (D03, D09, D17, D24, D51, and D92). The selected images are similar in greyscale distribution but represent clear differences in the texture appearance with and without directional dependency.

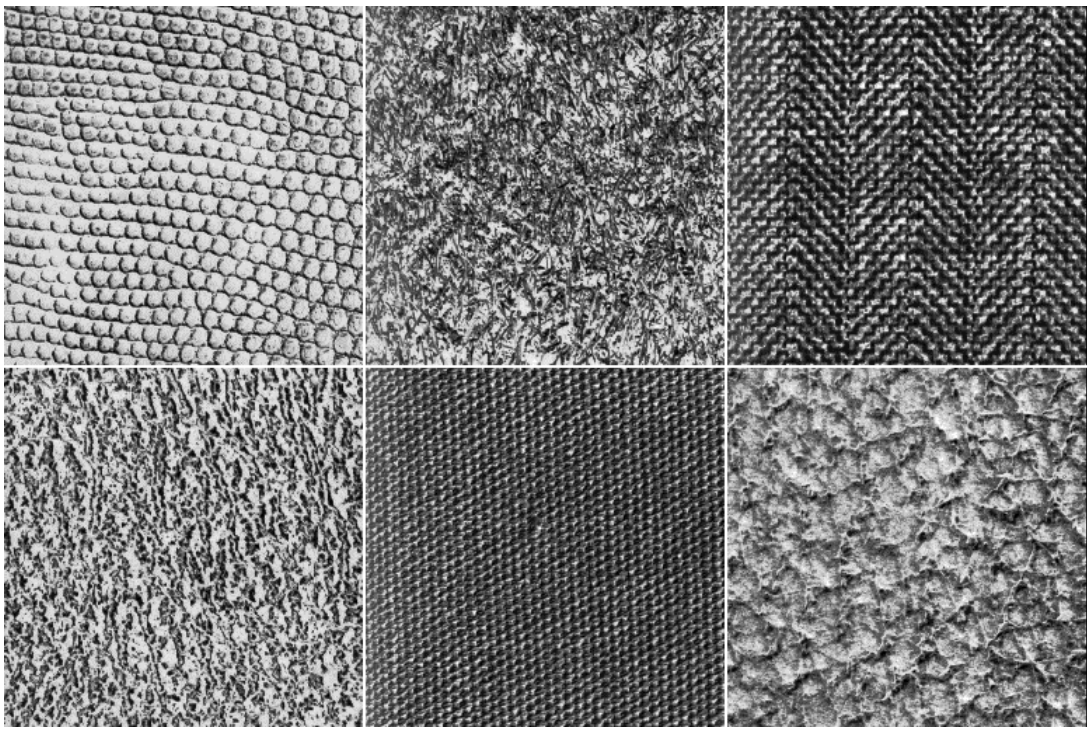

Figure 4. Brodatz natural textures used for application 2. Top row: B03, B09, B17. Bottom: B24, B77, B92.

Each of the six images is split into sixteen equally large regions of size 64×64. *MA* and *MY* are calculated for all four modes with *s* ranging from 1 to 50 in steps of 1 and *N*=1000. *MA* and *MY* are appended to account for a specific dimension. Thus, the entire data for Mode 0 and Mode 1 consist of 96×2×50 data points. Mode 2 and Mode 3 consist of 96×2×4×50 data points, because four different values of β and γ are used, respectively. These multivariate data set are decomposed using the Tucker method, and the score values of the decomposition are plotted in Figure 5a-d to display the discriminative ability of the AMT texture features.

Figure 5a shows the score values of the two first components of the Tucker decomposition of the Mode 0. A reasonable separation with the AMT features of the B17, B24, and B77 images is observed. The remaining texture measures are overlapping and especially between B03 and B09 there is a high degree of overlap. The reason for this is the inhomogeneity of the B03 texture observed in Figure 4.

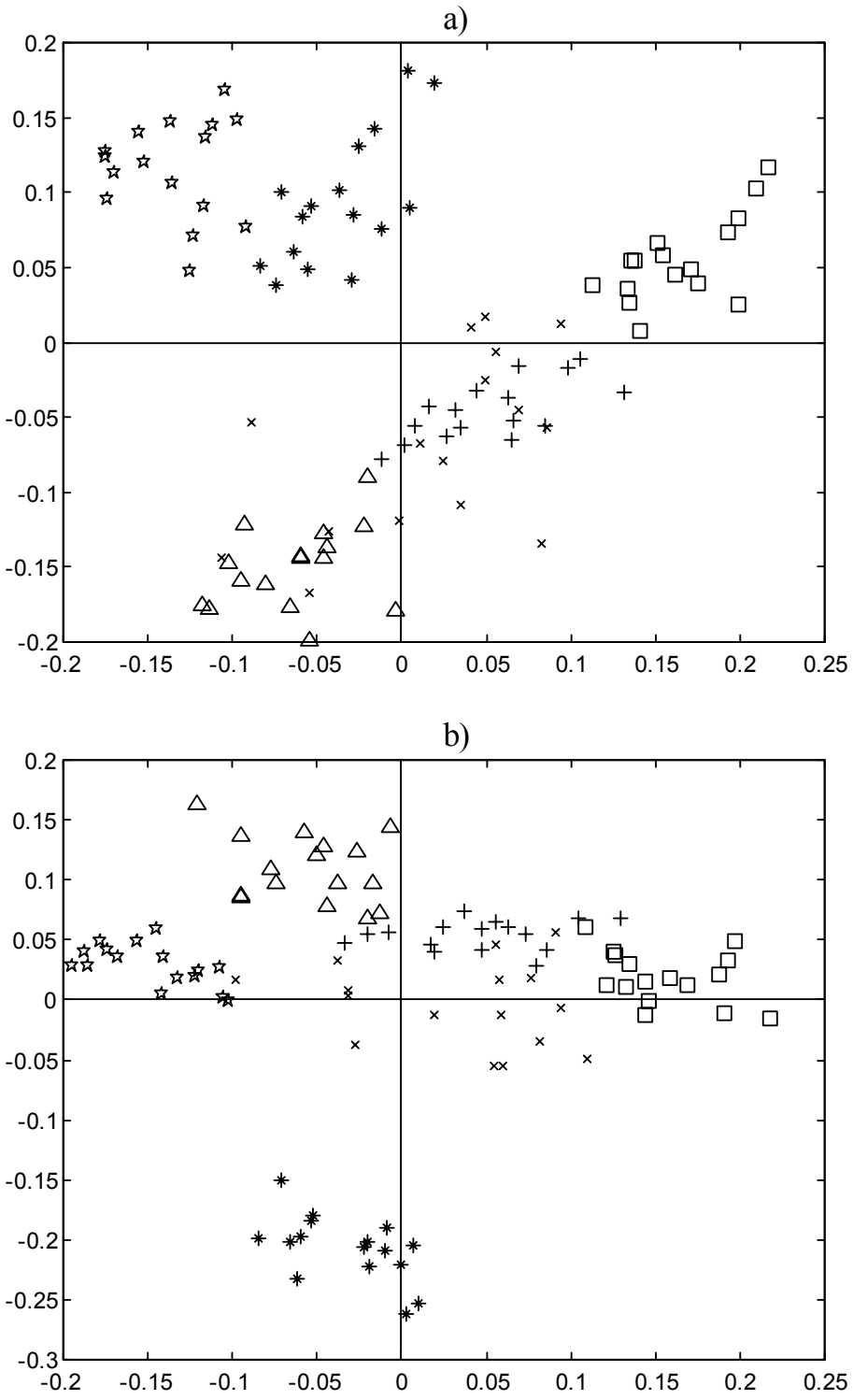

Figure 5. Continued.

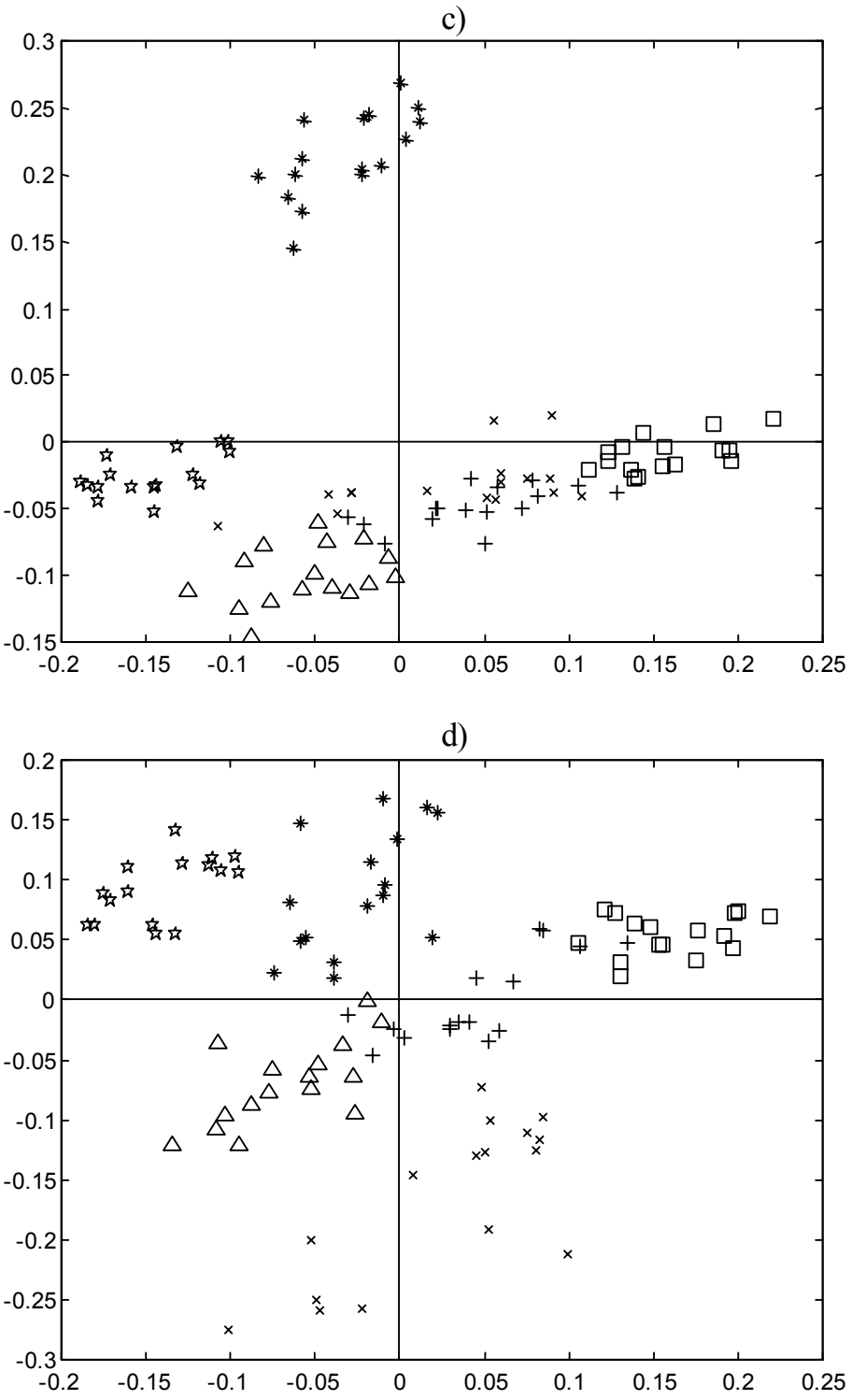

*Figure 5. Scatterplot of the scores from the first two components of the Tucker decomposition of the AMT data measured on the Brodatz images. a) Mode 0. b) Mode 1. c) Mode 2. d) Mode 3. The 16 replicates from each of the Brodatz images are marked with the following symbols: B03: ×, B09: +, B17: *, B24:□, B77: ★, and B92: Δ.*

The classification of the Brodatz textures with the Mode 1 AMT is shown in Figure 5b. The separations between the six textures have improved compared to the Mode 0 measurements. The B17 class is widely separated from the remaining by the decomposed component two. Also B24, B77 and B92 seem to be grouped closer within each class compared to Mode 0. The problem with the overlap of the B03 is smaller than for Mode 0 but still present. Except for a few overlaps with B03, the B09 class is almost separated from the remaining samples with the Mode 1 approach.

The Mode 2 classification is shown in Figure 5c. Generally the same characteristics as previous are observed: B17 is clearly separated from the remaining samples, and B24, B77, and B92 are fairly well separated from the remaining samples, and the three clusters tend to be grouped closer than for Mode 1. Similar to the Mode 0 results, the B03 and B09 features are largely overlapping.

The result of the Mode 3 decomposition is shown in Figure 5d. The B17 texture is not as separated for the Mode 3 approach as for the Mode 1 and the Mode 2 AMT. Yet the class is still separated from the remaining classes, as also the B24 and B77 samples are seen to be. The B03 texture measures are spread over a fairly wide area due to the inhomogeneity of the texture patterns. However, the B03 class is separated from the remaining clusters of textures, which have not been seen for the remaining modes. However, the B09 texture measures are observed to overlap slightly with the B24 and B92 groups. Despite of this overlap, the Mode 3 grouping seems to be presenting the generally best variation between the groups.

The results presented in application 2 could most likely be improved by imposing a true classification approach on the problem. It is, for instance, likely that using more than two decomposition components will separate the B03 and B09 samples in Mode 2. However, the approach followed here illustrates a rapid initial screening of a texture classification problem with the AMT without an advanced parameter optimisation. The illustrated approach is very much explorative, and can help isolate the core of the segmentation process with a minimal effort.

APPLICATION 3. INTRAMUSCULAR FAT IN ULTRASOUND IMAGES

A third application, prediction of intramuscular fat (IMF) in ultrasonic images, is presented. The ultrasound information is measured with the Autofom system, which is an automated system for grading of pork carcasses. The system performs a three-dimensional scanning of the carcass with 16 transducers positioned evenly over the back of the carcass. For every 5 mm (approximately 100 mm in total) each transducer scans a depth of 110 mm with a resolution of 0.15 mm. Totally the scanning therefore consist of 16×200×600 measured points. For more information of the Autofom system, see Brøndum *et al.*[23]. IMF is believed to be detectable with the ultrasonic information due to speckle effects in the ultrasonic data. The representation of the IMF speckle is thus dependent on the ultrasonic resolution, and the coarse resolution

in the longitudinal direction of the Autofom (0.5 mm) is a potential problem. Therefore, a part of the trial was set up to measure the carcasses at reduced line speed and with an increased longitudinal resolution. With the low resolution, the selected region of 100×60 pixels covers an area of 100×20 mm. In the test with the high resolution, the selected region cover an area of 200×20 mm. Figure 6 shows two longitudinal ultrasound images acquired by one of the transducers (16 such images exist for each carcass). Figure 6a is with the normal line speed and Figure 6b is with the reduced line speed. The squared white regions marked on the images denote the location of the areas of interest for the IMF. The regions are selected manually, but automatic selection should be trivial to implement due to the location of the ribs just above the selected region.

Fourty-five carcasses are measured with the normal resolution and 48 carcasses are measured with high resolution. Upon dissection of the carcasses, meat samples of approximately 200 g were cut at the 10^{th} rib and scored by a meat inspector from 1 to 5 according to the visual evaluation of the marbling following the NPPC procedures[24], except that also half digit scores are used. The samples were then sent to a laboratory for chemical extraction of lipids. The two reference parameters describe quite different information in the meat samples. The marbling score is a surface evaluation and the lipid extraction is a measure for the entire sample. The correlation coefficients between the two measures are 0.61. Statistic parameters for the two reference parameters are shown in Table 1.

Table 1. Statistic parameters for the reference parameters lipid extraction and marbling score.

	Mean	SD	Max	Min
Lipid	5.50	2.88	13.9	1.57
Marbling	2.25	0.89	4.0	1.0

MA and *MY* are measured with Modes 0-3. The AMT spectra were averaged over 1000 measurements and *s* were varied from 1 to 60 in steps of 1. *MA* and *MY* for Mode 3 are shown in Figure 7 for two relatively extreme samples with lipid values of 2.07% and marbling scores of 1.5 (Figure 7a,b) and 8.55 % and marbling scores of 3.5 (Figure 7c,d). The difference between the AMT data for the two samples is pronounced. *MA* in Figure 7a is exponentially declining with the scale value, whereas *MA* in Figure 7c appears to contain more noise due to the higher scatter effect in the ultrasound images. This effect is also depicted in the difference in the *MY* data, where the different γ-values show distinct contrast for the two samples. Also the *MY* level is different for Figure 7b and d. This justifies for the prediction of the reference parameters of with the AMT data.

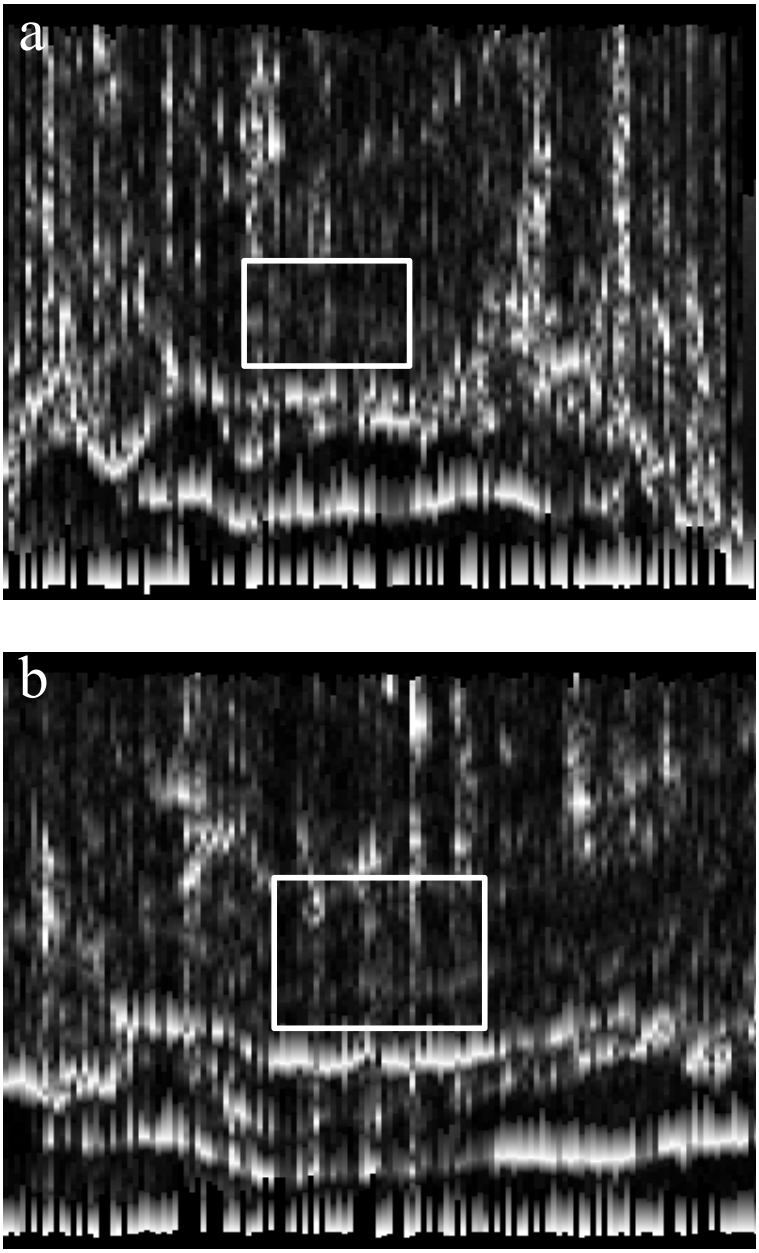

Figure 6. Autofom ultrasound image. The white squared region marks the area where the intramuscular fat is detected. a) Normal resolution. b) High resolution.

The AMT data for the four modes are used to predict the lipid and the marbling information with N-PLS. Twenty samples are selected randomly for the test set and the remaining samples (25 for the normal resolution and 28 for the high resolution) are used for the calibration set. Table 2 presents the correlation between the measured and the predicted for four modes.

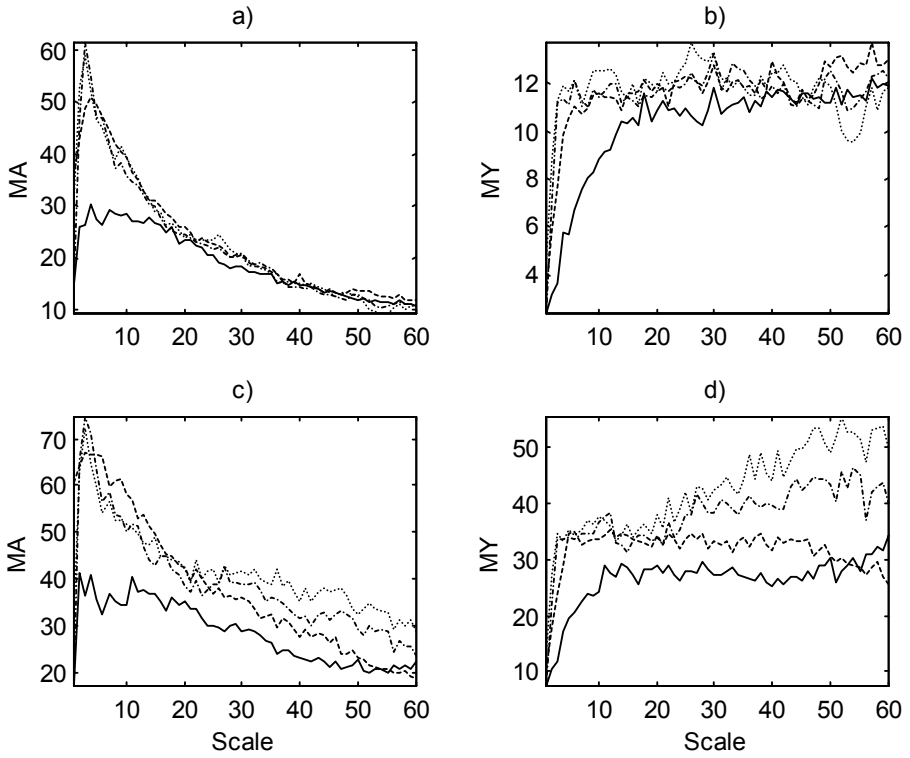

Figure 7. AMT Mesh plot of AMT Mode 3 the Autofom images of two extremes. a and b are from an animal with IMF of 2.07% and c and d are from an animal with IMF of 8.55%.

Table 2. Correlation coefficients (r) between the measured IMF values and the predicted with N-PLS for the normal and the high ultrasound image resolutions.

	Mode 0		Mode 1		Mode 2		Mode 3	
	Lipid	Score	Lipid	Score	Lipid	Score	Lipid	Score
Normal Resolution	0.44	0.47	0.49	0.56	0.51	0.50	0.50	0.57
High Resolution	0.79	0.63	0.75	0.69	0.81	0.68	0.81	0.71

As seen from Table 2, the high resolution images are far better for evaluating the IMF, which is no surprise. The normal resolution performance is doubtful to be useful for on-line sorting. Mode 2 and Mode 3 tend to be superior to Mode 0 and Mode 1, and especially the Mode 3 results are very encouraging for further work. The measured lipid versus the predicted with the Mode 3 AMT is shown in the scatterplot in Figure 8.

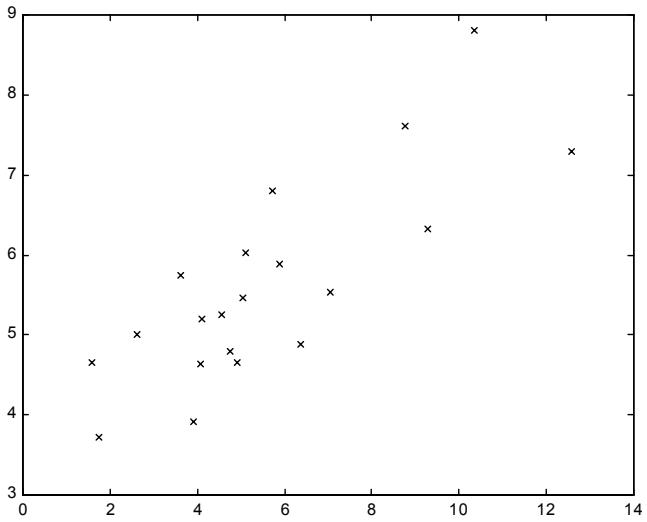

Figure 8. The measured lipid values versus the predicted with the Mode 3 AMT.

For comparison, also Grey Level Co-occurrence Matrix (GLCM) features were calculated[6]. The GLCM features were the 2nd, 3rd, 5th, 7th moments, maximum index, and entropy. The features were measured with a neighbouring distance of 5 pixels and they were measured with the neighbouring angles 0°, 45°, 90°, and 135°. This also results in a two-dimensional data structure with orientation information, which can be immediately input into the N-PLS regression method. Correlation values between the predicted ad the measured reference information for the high resolution images were 0.79 for the lipid extract and 0.64 for the marbling scores. Thus, the results obtained were very comparable to the Mode 0 prediction results and slightly poorer than the results obtained with the Mode 2 and Mode 3 AMT measures.

Due to indirect relations between the IMF and the carcass composition, further improvements in the predictions are likely to be reached by including the existing Autofom parameters. This cannot be tested in the current trial because the reduced line requires extensive software changes of the on-line system. However, preliminary test with manual reading of the Autofom images indicate that a further improvement of approximately 6% can be reached by including indirect information of the fat depth, the meat depth, and the thickness of the individual fat layers. This indication supports the potential use of the Autofom for on-line quality measurement of IMF for sorting on the abattoir. The use of AMT in the on-line system is a realistic possibility. Currently, approximately 1.0 s is used for a Mode 0 or Mode 1 measurement and 3.5 s is used for a Mode 2 or 3 measurement on a SGI Indy 4600SC (Silicon Graphics, CA, US). Further improvement of the implementation and upgrade of the hardware will enable on-line use of the AMT at the required abattoir line speed.

The results obtained for the AMT and N-PLS predictions are encouraging for further work with the high resolution Autofom data. Surely, the data presented here are not of sufficient quantity to justify for an immediate implementation, but the indications observed are positive. The results are the first presented on porcine meat, but the experiences are similar to those obtained by e.g. Herring *et al.*[25] on beef meat, which reported correlation values of 0.61 and 0.75. The higher correlation for the lipid extracts obtained in this study, are believed to reside in the higher variation in this data, which was sd=2.88 versus sd=2.25 for Herring *et al.*[25]. The prediction level appears to be sufficient for introducing an automatic coarse sorting of the quality extremes in the abattoirs, which is currently not possible. It is doubtful whether further improvements in the image resolution also will improve the predictions. There is an upper limit of the accuracy of the reference information represented by the chemical extracts and the visual scores, and in the further work attention should also be kept on this matter.

DISCUSSION

The major advantage of the AMT is that the texture information is tranformed into the scale domain. This makes AMT a very robust and generalised approach to measurement of texture pattterns, which can be applied to both segmentation and prediction problems. The use of the scale domain also enables the comparison of images or signals from different domains and image sizes can be compared.

Another of the major advantages of AMT is that it requires practically no parameter optimisation. The only parameters necessary in the AMT method is the number of averages, which have no influence on the data when the AMT measures becomes deterministic, and the *s* start and stop positions and stepwise increase, which have little influence on the succes of the AMT output due to the collinear struture of the data. Thus, the usual problems of optimising the scale dependency is removed from the texture operation. Often, much time is spend on optimising the application to function on a specific texture pattern. Here, AMT have been used in three very different applications with success with the same parameter use. When combining the AMT data with multivariate decomposition techniques, this approach possesses the possibility to establish a very strong fundamental utility for rapid and general screening in texture studies.

The advantage of the generalisation of the AMT method does, however, also tend to be the disadvantage of the system. Parameter optimisation can often be used to tune texture algorithms in to match specific textures precisely. It is therefore not unlikely that AMT can be outperformed by other methods in very specific cases.

The AMT is non-recursive in contrast to e.g. the Fourier transformation. Thus, the scale domain can thus not be used for textures with specific scale domain properties and the retransform to the spatial domain. A similar result can be obtained by removing the random selection of the origo point, and instead perform the angle measure for each pixel. This naturally requires an extensive increase of processing time, but this can be remedied by increasing the scale steps.

The two-dimensional AMT introduced here possesses some theoretical advantages in the utilisation of the image information, which can easily be extended to higher number of dimensions. The practical advantages of the two-dimensionality in the AMT are apparent for both the classification of the Brodatz images and the prediction of IMF from the ultrasonic images.

In the current implementation Mode 0 and Mode 1 are calculated on 1.0s and Mode 2 and Mode 3 are calculated on 3.5s with N=1000 and 60 scale values on a SGI Indy 4600SC (Silicon Graphics, CA, US). No special attention has been made to speed optimisation of the algorithm, and improvement of at least a factor 2 can be expected if required. This should make the AMT measures an interesting approach for most texture analysis systems with respect to the processing time.

SUMMARY

The angle measure technique (AMT) was proposed for use in geometric land characterisation by Andrle[9] and was proven to be superior to fractal dimension for this purpose. Esbensen *et al.*[10] picked up the technique for image texture analysis and worked on unfolded images, an approach which was denoted Mode 0 in this paper. AMT transforms α defined as the angle between two vectors $\overline{OA}$ and $\overline{OB}$ of length *s*, where O is a moving origo and A and B are moving points in the image. The angles between the two vectors are transformed into a scale domain with *s* as the dependent variable. By varying the scale value s and averaging the angle over N repetitions, a mean angle (*MA*) are found. Since the further data processing is performed in the scale domain, AMT automatically accounts for scale and magnification differences in the texture. Esbensen also proposed to use the mean difference of the intensities (*MY*) between the outer border points (A, B) in the scale domain. In this paper, AMT has been extended to two dimensions in the selection of the origo and the outer border points. Three approaches for this are proposed: random sampling (Mode 1), direction independence (Mode 2), and rotational independency (Mode 3). These have been implemented by selecting the points O, A, and B in the spatial domain under constraints for the angle between vectors $\overline{OA}$ and the horisontal direction, β, and the angle between the vectors $\overline{OA}$ and $\overline{OB}$, γ. This has introduced an angle dimension in

the scale domain and called for multi-way data evaluation. The nature of the two-dimensional AMT data were illustrated by a simple 2D sinusoid image. To demonstrate the classification ability of the AMT features, a decomposition to two common factors has been introduced with the Tucker decomposition[15,16]. The efficiency of the AMT data combined with the Tucker decomposition was illustrated on the Brodatz natural textures. Almost a complete separation of small subregions of 6 natural textures was observed using only two decomposed factors despite a clear texture variation for especially one of the textures. The predictive ability of the AMT features was demonstrated on an trial where intramuscular fat are predicted from ultrasonic images of pork carcasses. AMT was slightly superior to 7 GLCM features extracted in four directions and used in a multi-way partial least squares regression.

The main advantages of the AMT tend to be threefold: 1) the generalisation and nonessential parameter optimisation makes the approach an easy to use tool for empirical texture screening. 2) The scale domain makes the AMT when combined with e.g. multivariate decomposition facilitates an internal correction for changes in scale and magnification. 3) The possibility of mapping texture information from images (or signals) from different sizes and even different dimensions onto the same domain for comparison. The disadvantage of the AMT seems to be the lack of reversibility and the generalisation, where the low optimisation facility makes it hard to optimise the texture information measured with AMT on a specific solution. Much more work, however, still remains to be made with this interesting novel texture technique.

REFERENCES

[1] M.E. Jernigan and F. D'Astous, Entropy-based texture analysis in the spatial frequency domain *IEEE Transactions on Pattern Analysis and Machine Intelligence*, vol. 6, pp. 237-243, 1984.

[2] D. Dunn, W.E. Higging, and J. Wakeley, Texture Segmentation Using 2-D Gabor Elementary Functions *IEEE Transactions on Pattern Analysis and Machine Intelligence*, vol. 16, pp. 130-149, 1994.

[3] K.I. Laws, Textured image segmentation *USCIPI Rep.940, Image Processing Inst., University of South.Ca., LA*, vol. 1980.

[4] A.P. Pentland, Fractal-based description of natural scenes *IEEE Transactions on Pattern Analysis and Machine Intelligence*, vol. 6, pp. 661-674, 1984.

[5] C.S. Lu, P.C. Chung, and C.F. Chen, Unsupervised texture segmentation via wavelet transformation *Pattern Recognition*, vol. 30, pp. 729-742, 1997.

[6] R.M. Haralick, K. Shanmugan, and I. Dienstein, Textural Features for Image Classification *IEEE Transactions on Systems, Man and Cybernetics*, vol. 3 , pp. 610-621, 1973.

[7] J.M.H.d. Buf, M. Kardan, and M. Spann, Texture feature performance for image segmentation *Pattern Recognition*, vol. 23, pp. 291-309, 1990.

[8] T.R. Reed and J.M.H.d. Buf, A review of recent texture segmentation and features extraction techniques *CVGIP: Image Understanding*, vol. 57, pp. 359-372, 1993.

[9] R. Andrle, The Angle Measure Technique: A New Method for Characterizing the Complexity of Geomorphic Lines *Mathematical Geology*, vol. 26, pp. 83-97, 1994.

[10] K. Esbensen, K. Hjelmen, and K. Kvaal, The AMT Approach in Chemometrics - First Forays *J.of Chemometrics*, vol. 10, pp. 569-590, 1996.

[11] K. Kvaal, J.P. Wold, U.G. Indahl, P. Baardseth, and T. Næs, Multivariate feature extracton from textural images of bread *Chemometrics and Intelligent Laboratory Systems*, vol. 42, pp. 141-158, 1998.

[12] K. Kvaal, P. Baardseth, U.G. Indahl, and T. Isaksson. Relationships between sensory measurements and features extracted from images. In: *Multivariate Data Analysis in Sensory Science*, eds. T. Næs and E. Risvik. Elsevier Science B.V., 1996.pp. 135-157.

[13] H. Martens and T. Næs. *Multivariate Calibration*, Wiley, New York, 1993.

[14] K.H. Esbensen and P. Geladi, Strategy of multivariate image analysis (MIA) *Chemometrics and Intelligent Laboratory Systems*, vol. pp. 67-86, 1989.

[15] R. Bro, Multi-way analysis in the food industry. Models, algorithms and applications 1998. Doctoral Thesis. Chemometrics Group, Food Technology, KVL, Copenhagen, Denmark.

[16] R. Henrion, N-way principal component analysis. Theory, algorithms and applications *Chemometrics and Intelligent Laboratory Systems*, vol. 25, pp. 1-23, 1994.

[17] L.R. Tucker. Implications of Factor analysis of three-way matrices for measurement of change. In: *Problems of Measuring Change*, ed. C.W. Harris. Univ. Wisconsin, Madison, *MA*, 1963.pp. 122-137.

[18] L.R. Tucker, Some mathematical notes on three-mode factor analysis *Psychometrika*, vol. 31, pp. 279-311, 1966.

[19] R. Bro, Multiway calibration. Multilinear PLS *J.Chemometrics*, vol. 10, pp. 47-61, 1996.

[20] C.R. Rao and S. Mitra. *Generalized inverse of matrices and its applications*, Wiley, New York, 1971.

[21] P. Brodatz. *Textures*, New York, Dover, 1966.

[22] H. Greenspan, R. Goodman, R. Chellappa, and C.H. Anderson, Learning Texture Discrimination Rules in a Multiresolution System *IEEE Transactions on Pattern Analysis and Machine Intelligence*, vol. 16, pp. 894-901, 1994.

[23] J. Brøndum, M. Egebo, C. Agerskov, and H. Busk, Carcass Grading with the Autofom Ultrasound System *J.Anim.Sci.*, vol. 51, pp. 1859-1868, 1998.

[24] NPPC, Procedures to evaluate market hogs. National Pork Producers Council, des Moines, IA, USA, 1991.

[25] W.O. Herring, L.A. Kriese, J.K. Bertrand, and J. Crouch, Comparison of Four Real-Time Ultrasound Systems That Predict Intramuscular Fat in Beef Cattle *J.Anim.Sci.*, vol. 76, pp. 364-370, 1998.